energies

MDPI

Article

Nickel Hydroxide Nanofluid Cathodes with High Solid Loadings and Low Viscosity for Energy Storage Applications

Sujat Sen [1,*], Elahe Moazzen [2,3], Sinjin Acuna [4], Evan Draxler [1], Carlo U. Segre [3,4] and Elena V. Timofeeva [2,4]

[1] Department of Chemistry and Biochemistry, University of Wisconsin La Crosse, La Crosse, WI 54601, USA; draxler8058@uwlax.edu
[2] Department of Chemistry, Illinois Institute of Technology, Chicago, IL 60616, USA; emoazze@hawk.iit.edu (E.M.); etimofeeva@influitenergy.com (E.V.T.)
[3] Department of Physics & CSRRI, Illinois Institute of Technology, Chicago, IL 60616, USA; segre@iit.edu
[4] Influit Energy, LLC, Chicago, IL 60612, USA; sacuna@hawk.iit.edu
* Correspondence: ssen@uwlax.edu

Abstract: Nanofluid electrodes with high loading of active solid materials have significant potential as high energy density flow battery electrolytes; however, two key criteria need to be met: they must have a manageable viscosity for pumping and simultaneously exhibit good electrochemical activity. A typical dispersion of nickel hydroxide nanoparticles (~100 nm) is limited to 5–10 wt.% of solids, above which it has a paste-like consistency, incompatible with flow applications. We report on the successful formulation of stable dispersions of a nano-scale nickel hydroxide cathode (β-$Ni(OH)_2$) with up to 60 wt.% of solids and low viscosity (32 cP at 25 °C), utilizing a surface graft of small organic molecules. The fraction of grafting moiety is less than 3 wt.% of the nanoparticle weight, and its presence is crucial for the colloidal stability and low viscosity of suspensions. Electrochemical testing of the pristine and modified β-$Ni(OH)_2$ nanoparticles in the form of solid casted electrodes were found to be comparable with the latter exhibiting a maximum discharge capacity of ~237 mAh/g over 50 consecutive charge–discharge cycles, close to the theoretical capacity of 289 mAh/g.

Keywords: nanofluids; low viscosity; nickel hydroxide; nanoelectrofuels; flow battery

check for updates

Citation: Sen, S.; Moazzen, E.; Acuna, S.; Draxler, E.; Segre, C.U.; Timofeeva, E.V. Nickel Hydroxide Nanofluid Cathodes with High Solid Loadings and Low Viscosity for Energy Storage Applications. *Energies* **2022**, *15*, 4728. https://doi.org/10.3390/en15134728

Academic Editor: Senentxu Lanceros-Mendez

Received: 27 May 2022
Accepted: 23 June 2022
Published: 28 June 2022

Publisher's Note: MDPI stays neutral with regard to jurisdictional claims in published maps and institutional affiliations.

Copyright: © 2022 by the authors. Licensee MDPI, Basel, Switzerland. This article is an open access article distributed under the terms and conditions of the Creative Commons Attribution (CC BY) license (https://creativecommons.org/licenses/by/4.0/).

1. Introduction

Engineered nanoparticle suspensions, known as "nanofluids", have been extensively studied in the last decades due to their potential applications as advanced heat transfer fluids [1–6] and are steadily gaining interest for their energy storage capabilities [7–13]. These nanofluids combine some of the advantages of solid and liquid phases. Liquids are flowable, conformable in shape and have convective mechanisms for energy, mass, and momentum transfer. Solids dispersed inside nanofluids can provide novel functionality but also change fluid dynamics, viscosity, thermal conductivity, density and specific heat [14–20].

Nanofluids containing electrochemically active nanoparticles have the form of suspension electrodes [21–24], where the electron transfer occurs when freely suspended particles undergo collisions with an electrically polarized current collector [25,26]. Nanofluid electrodes containing high energy density battery anode and cathode nanoparticles can be used in flow batteries replacing traditional anolytes and catholytes [27] and have been named nanoelectrofuels [28]. Since nanoelectrofuels are not limited by solubility considerations, they can theoretically achieve much higher energy storage capacity when compared to traditional flow battery electrolytes [29]. Nanoelectrofuels effectively combine the high energy density of solid-state battery materials with the operational flexibility of redox flow batteries, thereby producing a new high energy density pumpable battery format [26,28]. As nanoelectrofuels are a liquid, they can be pumped to and from the battery stack for

continuous charge and discharge cycles, while being stored in external tanks. This decoupled format allows for independent power and energy storage characteristics through the independent sizing of the power stack and storage tanks (akin to traditional designs for a flow battery). On the other hand, for solid-state systems, power, storage capacity and packing scale linearly with the size of the battery.

The concept of suspension electrodes was demonstrated over three decades ago for catalysis [21,30], but only recently have they been considered as prospective flow battery electrolytes. One of the first reports of suspension electrodes for flow battery applications involved Li-based slurries composed of micrometer-sized particles mixed with a conductive carbon additive that also served as a support structure [31,32]. Charging and discharging of the battery were achieved during the extrusion of the high viscosity electrode material through the flow battery half-cells. Other studies have explored a similar concept for other electrochemical applications, including supercapacitors [33–36]. A common thematic challenge to this approach of electrochemically active fluidized electrodes has been the extremely high suspension viscosity of the composite (>1000 times higher than traditional flow battery electrolyte), which results in pumping power penalties, limited power ratings, limited discharge rate, and incomplete discharge resulting in extra cost, inactive battery weight, and limited efficiency. Hence, both viscosity and suspension stability must be addressed, especially for applications that rely on pumping.

Nanofluids are intrinsically more stable toward settling due to gravity since the Brownian motion of smaller particles effectively counteracts the sedimentation process. Hence, an additional support structure (e.g., conductive filler) is not necessary for stability against sedimentation. This enables the formulation of nanofluids with a high fraction of un-supported electrochemically active nano-sized particles with low viscosity [26]. Furthermore, nano-scale battery particles are known to have significantly faster charge–discharge rates due to shortened internal diffusion paths when compared to micron-sized particles of the same material [37]. Therefore, for the successful formulation of nanofluids as flowable suspension electrodes, the following criteria need to be met: (i) high fraction (e.g., >50 wt.%) of solid particles in suspension to achieve high energy density; (ii) low viscosity with minimal shear dependence for efficient pumping of the nanofluid, and (iii) good electrochemical activity towards charge and discharge reactions [26]. Achieving all of these functional needs in one formulation represents a significant engineering challenge [26,28]. We have recently demonstrated a rheology-oriented approach towards an electrochemically active fluidized electrode that uses stabilized suspensions of nanoparticles at high solid loading with manageable viscosities while retaining good electrochemical activity [38,39].

This study reports on the development of a cathodic nanoelectrofuel using Nickel hydroxide ($Ni(OH)_2$), which has been widely used as a battery material for aqueous batteries [40]. Nickel hydroxide and its dehydrated form, nickel oxide (NiO) has been explored in the literature for a variety of applications such as photocatalysis, [41] electrocatalysis [42], supercapacitors [43–47], electrochromic devices [48–51] and electrochemical sensors [52–54]. Furthermore, it has been identified to be a promising material for industrial applications given its cost effectiveness, abundant precursor chemicals and ease of synthesis [40,55]. In particular, its electrochemical properties have been widely investigated, forming the basis of commercial battery and supercapacitor technologies [40]. Under alkaline conditions, the Ni (II)/Ni (III) redox couple in $Ni(OH)_2/NiOOH$ provides a reversible theoretical capacity of 289 mAh/g.

Preventing the agglomeration of the nanoparticles [26,28] is the key to controlling the viscosity of nanofluids. Several approaches to achieving high solid loading of nano-sized particles in suspensions with modest viscosity have been previously reported in the literature. This includes the use of (i) surfactants that spatially separate particles to prevent their agglomeration or (ii) tailoring the charges of the particle surface via the use of customized electrolytes (pH, ionic strength); or (iii) surface grafting of small molecules [26]. While a variety of aqueous and non-aqueous fluids containing metal and ceramic particles have been studied for their rheological and other physicochemical

properties [4], the use of nickel hydroxide has been rather limited. Qazi et al. [56–58] report on the rheology of suspensions made using $Ni(OH)_2$ nanoplatelets (100 nm diameter with polyacrylate stabilizer), where a suspension with a concentration of 23 wt.% had a viscosity of 90 cP. Diffraction and neutron scattering techniques were used to study the alignment dispersions of plate-like colloidal particles of $Ni(OH)_2$. Higher concentrations up to 35 wt.% were prepared but not studied as they were deemed too viscous to obtain flow. Brown et al. [59,60], also reported a study of concentrated aqueous $Ni(OH)_2$ suspensions (hexagonal plates with 85 nm diameter stabilized by polyacrylates) of up to 62 wt.% in 20 mM NaCl. It exhibited shear-thinning behavior across a wide range of shear rates from 1000 cP at $1s^{-1}$ to 300 cP at a shear rate of 100 s^{-1}. Suspensions with higher concentrations up to 68 wt.% were prepared and reported to be "extremely viscous", but no rheological behavior was provided.

While a variety of reports exist in the literature, they typically introduce significant amounts of additives to achieve a practically acceptable viscosity. These surface modifying agents or additives are often not redox active and thus likely to have detrimental effects on the electrochemical performance [26]. Another approach to achieving modest viscosity of high solid loading suspensions is through the anchoring of small functional groups to the surface of nanoparticles [20]. Both steric and electrostatic features of a functional group can be used to achieve separation of particles resulting in higher suspension stability while minimizing detrimental effects on the electrochemical response of the nanomaterial. We have previously explored a similar approach for the formulation of nanoelectrofuels with titania [39] and iron oxide nanoparticles [26,38]. In both cases, surface-modified nanoparticles enabled significantly higher particle loadings and lower viscosity of nanofluids than unmodified nanomaterials. However, multiple layers of the surface graft were present at the nanoparticle surface, and the electrochemical activity of modified nanomaterials was partially suppressed [38,39].

In this study, we explore a chemical synthesis of nickel hydroxide nanoparticles and subsequent grafting of small organic molecules onto their surface to achieve modest viscosities of the resulting nanofluids. Nickel hydroxide nanoparticles were chosen given their relatively low-cost, established redox chemistry and prevalent use as battery cathode material in aqueous systems. Furthermore, we demonstrate that this surface modification process does not prevent electrochemical access to the nanoparticle bulk. Viscosity and thermal conductivity of the resulting $Ni(OH)_2$ nanofluids in aqueous electrolytes are presented and compared to theoretical models. Electrochemical performance of both pristine and modified nickel hydroxide in the form of solid-casted electrodes is also presented herein as a steppingstone toward the formulation of flowable suspension electrodes.

2. Materials and Methods

2.1. Materials and Characterization Techniques

Nickel (II) chloride (Sigma-Aldrich, Milwaukee, WI, USA), ammonium chloride (Alfa Aesar, Ward Hill, MA, USA), sodium dodecyl sulfate (SDS, Acros Organics, USA), and sodium hydroxide (Fisher) were used as purchased. Size and morphology were examined using scanning electron microscopy (SEM, Hitachi S-4700, USA). Samples for SEM analysis were prepared by preparing a highly dilute suspension of the nanoparticles in ethanol, agitating through ultrasonication and then drop-casting onto a silicon wafer, followed by air-drying, as previously reported [26]. Crystalline structure before and after surface modification was confirmed by X-ray powder diffraction (XRD, Bruker D2, Cu K-alpha source, 0.15406 nm), refined directly by EXPGUI, GSAS software using ICSD crystallographic information. Thermogravimetric (TGA) analysis (SDT Q-600, TA Instruments, New Castle, DE, USA) of the nano-powders before and after surface modification was conducted to quantify the amount of grafted material. In a typical test, a 10–15 mg sample was heated from 30 °C to 1000 °C at 10 °C/min rate under N_2 flow as per previously reported methods [26].

2.2. Synthesis of Nickel Hydroxide Nanoparticles

In total, 12.00 g $NiCl_2 \cdot 6H_2O$, 3.00 g sodium dodecyl sulfate (SDS), and 16.20 g NH_4Cl were dissolved in 600 mL of deionized water (molar ratio Ni^{2+}/NH_4^+ at 1:6). The solution was magnetically stirred at 700 rpm and heated on a hot plate to 60 °C. A solution of 10 M NaOH was added dropwise to raise the pH to 6.3 to achieve full complexation of $[Ni(NH_4^+)_6]^{2+}$. An additional ~36 mL of 10 M NaOH was then injected rapidly in one aliquot into the solution to raise pH to above 10 and induce rapid precipitation. The reaction mixture was then stirred for additional 2 hrs, maintaining temperature at 60 °C. The resulting $Ni(OH)_2$ nanoparticles (further referenced as pristine) were isolated by vacuum filtration, washed profusely with deionized water and ethanol, and dried under vacuum at 60 °C.

2.3. Surface Modification of Nickel Hydroxide Nanoparticles

3-(trihydroxysilyl)-1-propane sulfonic acid (40 wt.%, Gelest Inc., Morrisville, NC, USA), a commercially available graft, was used to allow a scalable process [26]. A total of 3 g of pristine nickel (II) hydroxide nanoparticles were mixed with 200 mL of absolute ethanol and 200 mL of deionized water and 1M NaOH solution as added dropwise to adjust the pH to 11. It was then sonicated in a bath for 4–6 hrs to ensure all the particles were well dispersed. A total of 4 g of 3-(trihydroxysilyl)-1-propane sulfonic acid was diluted in 20 mL of deionized water, and a 1 M solution of sodium hydroxide (NaOH, 98%, Fisher Scientific, USA) was added dropwise until pH reached 11. The two solutions were then mixed while stirring. The reaction mixture was then placed inside a sonic bath (37 kHz) and heated to 70 °C, while stirring mechanically (250 rpm). After 8 h, the system was transferred outside the sonic bath and kept stirring at 70 °C for an additional 16 h. The resulting sulfonated particles ($Ni(OH)_2$-S) were then isolated by vacuum filtration, washed profusely with deionized water and ethanol, and dried under vacuum at 60 °C.

2.4. Preparation of Nanofluids Using Dry Nanopowders

Aqueous solutions containing an overall hydroxide concentration of 40 mM (30 mM KOH and 10 mM LiOH) in Type-1 deionized (DI) water were used as base fluid in the preparation of all nanofluids. This serves as a representative electrolyte with salts and additives that are typically used in industrial processes and in alkaline battery electrolytes [53]. The requisite amounts of dry nanomaterial were added to the base fluid and mixed using alternating runs with the (i) vortex mixer (Fisher Scientific) and (ii) magnetic stirrer to achieve a homogeneous mixture. Following this, it was placed inside an ultrasonic bath for 4–6 h to achieve further dispersion and homogenization. In this study, nanofluid concentrations have been reported as a weight percent (wt.%). For example, 4 g of solids and 6 g of base fluid make 10 g of a 40 wt.% nanofluid. Interconversion factors of weight and volume percentages are presented in the supporting information (Figure S1).

2.5. Measurements of Nanofluid Properties

Before any testing, samples were re-agitated by ultra-sonication for at least 1 h. The dynamic viscosity of prepared fluids was measured using a Brookfield DV-II+ rotational-type viscometer with the SC4–18 spindle. The temperature range was maintained between 25 and 55 °C ± 0.2 °C using a recirculating temperature-controlled bath. Viscosity readings were taken over an average of 25 consecutive readings with variation of ± 2% at a shear rate of 264 s^{-1}, unless specified otherwise. A torque criterion of >10% and <90% was satisfied for all reported measurements, as per manufacturer recommendations. Agglomeration sizes of suspended nanoparticles were determined by dynamic light scattering measurements (DLS, Particle Size Analyzer, Zeta plus Brookhaven Instruments Corp., Holtsville, NY, USA). Samples for DLS were prepared by using a well-agitated 5 wt.% nanofluid and diluting with the base fluid to achieve <0.01 wt.% while retaining the same pH and ionic strength. Zeta potential measurements of both pristine and modified systems were conducted using dilute (<0.01 wt.%) fluids in 1.3 mM aqueous KOH, ensuring a pH of 10 and electrical

conductivity of approximately 400 µS. Thermal conductivity was measured on the basis of the transient hot wire method using a thermal property analyzer (KD2pro, Decagon Devices, Inc., Pullman, WA, USA) with a KS-1 probe with accuracy ± 5% for conductivities 0.2–2 W/mK. Reported measurements of thermal conductivity in this study represent an average value for 100 measurements taken at room temperature (21 ± 0.5 °C), with 15 min intervals. The typical standard deviation for the relative thermal conductivity increase values was <2%.

2.6. Electrochemical Testing

Electrochemical testing was conducted using solid casted electrodes as the working electrode, a nickel foam (1.6 mm thickness, MTI Corp., Richmond, VA, USA) as a counter electrode and an Hg/HgO reference electrode (CHI Instruments, calibrated to + 0.075 V vs. SHE at 298 K) in an aqueous solution of 5.5 M aqueous hydroxide containing both KOH and LiOH. Typically, 160 mg of the dry powder ($Ni(OH)_2$ or $Ni(OH)_2$-S), 20 mg of polyvinyl difluoride (PvdF, binder) and 20 mg of acetylene black (conductive filler) were mixed with N-Methyl Pyrrolidone (solvent), ensuring mixing through repeated cycles of vortex mixing and ultrasonication (37 kHz, 100% power, Fischerbrand 1122). It was then mixed overnight at 1000 rpm for 720 min, with two 1/8″ stainless steel milling balls (McMaster Carr) in a vortex mixer (Fischer Scientific). The black color paste was then painted onto pre-cut, weighed, 1 × 2 cm pieces of Nickel foam. After drying the electrode in a vacuum oven at 60–80 °C overnight, they were weighed again to determine mass loading. After a calendaring process, their net thickness was reduced to ~0.1 mm and then subjected to electrochemical tests [26,38]. A theoretical capacity of 289 mAh/g was used for all calculations of the Ni (II)/Ni (III) redox couple based on reaction stoichiometry of one electron transfer. A typical electrode contained a total of 25.6 mg material (with 80% active mass) spread across the current collector, resulting in a total capacity of 5.925 mAh (20.5 mg * 289 mAh/g). A C/3 charging rate used herein effectively means a current of 1.97 mA spread across 1 cm^2, i.e., a current density of ~2 mA/cm^2 or gravimetric current density of ~0.1 A/g.

3. Results

3.1. Surface Modification of Nickel Hydroxide Nanoparticles

Nickel hydroxide nanoparticles were synthesized by the two-step procedure mentioned in the experimental section, resulting in platelet-like nanoparticles with average sizes of 100–150 nm (length) × 25 nm (width), as shown in Figure S2. Rietveld refinement of the XRD data showed a grain size of 72 × 22 nm, consistent with the SEM data. The surface grafting procedure resulted in the nickel hydroxide nanoparticles with modified surfaces ($Ni(OH)_2$-S) containing negatively charged functional (sulfonate) groups $(Ni\text{-}O)_3\text{-}Si\text{-}(CH_2)_3\text{-}SO_3^-$ on the surface. The XRD diffractograms of nanopowders before and after the surface modification confirmed the β-$Ni(OH)_2$ phase. Furthermore, no major changes suggest that surface modification did not affect the crystalline structure of the material (see Figure S3, supporting information).

Thermogravimetric analysis (TGA) of pristine ($Ni(OH)_2$) and surface-modified nanoparticles ($Ni(OH)_2$-S) is shown in Figure 1a. Between 25 °C and 200 °C, both $Ni(OH)_2$ and $Ni(OH)_2$-S exhibited a small (<1%) change in mass, which can be attributed to the loss of physiosorbed water. Extended heating in the 200–600 °C range exhibited a steep weight loss of ~24 wt.% in the $Ni(OH)_2$ sample, likely due to the combined loss of any remaining surfactant molecules (SDS) used in the synthesis protocol, with simultaneous conversion to nickel oxide (NiO). Based on the thermal decomposition of nickel hydroxide (92.7 g/mol) to nickel oxide (74.6 g/mol), and water (with 1:1:1 stoichiometry, Equation (1)), we estimate a theoretical weight loss of 19.5 wt.% for pure nickel hydroxide.

$$Ni(OH)_2 \rightarrow NiO + H_2O \quad (1)$$

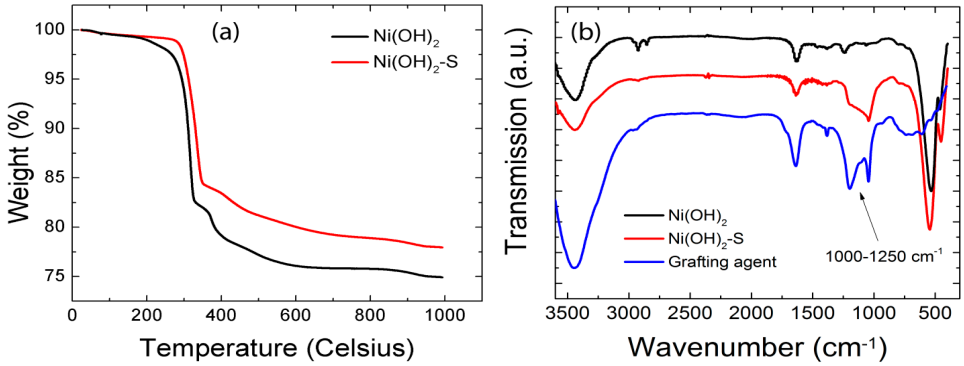

Figure 1. (**a**) TGA and (**b**) FTIR of pristine ($Ni(OH)_2$) and sulfonated nickel hydroxide nanoparticles ($Ni(OH)_2$-S).

However, the observed 24% weight loss instead suggests there is ~4.6 wt.% of surfactant (SDS) present in the pristine sample. Note that this surfactant content was present even after repetitive washing of the freshly synthesized nanoparticles, likely adsorbed due to electrostatic forces. The sulfonated nanoparticles exhibited a similar weight loss with a delayed onset for the initial steep mass loss. Final weight change after 600 °C was approximately 22%, indicating a net difference of approximately 2.6 wt.%, now attributed to the surface grafted moiety. This quantification of the surface graft present in the nanomaterial assumes that the surface modification procedure completely removes any residual SDS (surfactant) and replaces it with the silane-based graft. Additional tests with complementary methods would be needed to further confirm these results. Additional confirmation of the graft attached to the surface of the nanoparticle is obtained from FTIR spectra and is shown in Figure 1b. The spectra of modified nanoparticles and pure grafting agent show distinct peaks for Si–O and Si-metal bands in the 1000–1250 cm^{-1} range, confirming the presence of the grafting moiety in the surface-modified sample. The pristine $Ni(OH)_2$ powder has no specific features in this region. Our results suggest a substitution of electrostatically adsorbed SDS surfactant for chemically grafted surface-modifying graft at roughly a 1:1.2 atomic ratio, based on the TGA difference in mass loss (4.6 g vs. 2.6 g) and molecular weight of the surfactant (288 g/mol) and the surface modifier (202 g/mol).

3.2. Rheology of Nickel Hydroxide Nanofluids

Viscosities of the pristine ($Ni(OH)_2$) and sulfonated ($Ni(OH)_2$-S) nanofluids were measured at room temperature as a function of nanoparticle loading. Figure 2a reports viscosity relative to the base fluid as a function of solid weight fraction. Nanofluids with pristine $Ni(OH)_2$ nanoparticles were found to be stable against sedimentation with modest viscosities at a solid loading of 5 wt.%. Suspensions with higher concentration were found to have paste-like consistency at 10 wt.% (or 2.6 vol.%) and viscosity in excess of 2500 cP. Nanofluids with the surface-modified $Ni(OH)_2$-S nanoparticles had a significantly lower viscosity even at particle loadings as high as 60 wt.% (or 26 vol.%). Furthermore, they were found to be stable with no visible sediments after the viscosity measurement.

Figure 2a shows that the nanofluids made using pristine $Ni(OH)_2$ have a rapid, nonlinear increase in viscosity at solid loadings above 10 wt.%, while in the suspensions of $Ni(OH)_2$-S, a gradual, linear change in viscosity is observed with rapid increases seen above 50 wt.% solid loadings. Figure 2b shows that the viscosity of the nanofluid suspensions also decreases as a function of increasing temperature for all tested solid loadings. A nanofluid with 60 wt.% (26 vol.%) solids had a viscosity of 32 cP at room temperature and was found to be the highest experimentally achievable loading using $Ni(OH)_2$-S in this study. This value of viscosity is considerably smaller than several literature reports of $Ni(OH)_2$ nanofluids prepared under similar conditions. Most notably, this value can be closely compared to the work by Brown et al. [59,60], on 62 wt.% concentrated $Ni(OH)_2$ suspensions using hexagonal plates (85 nm diameter) stabilized by polyacrylates of up to

62 wt.% in 20 mM NaCl (the exact weight fraction of the stabilizer (polyacrylate) was not specified). Their suspensions exhibited a viscosity of 300 cP at a shear rate of 100 s^{-1}. Our approach to the formulation of concentrated nanofluids, reported in this paper, offers a 10-fold lower viscosity.

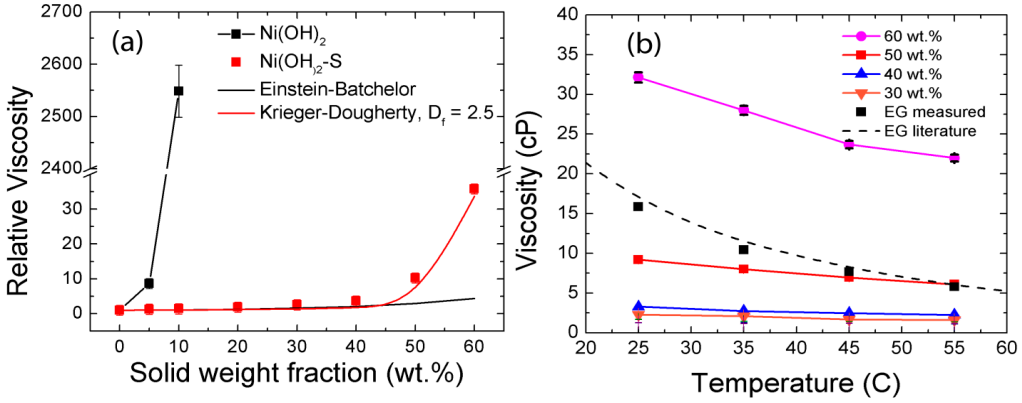

Figure 2. (**a**) Relative viscosity of nanofluids prepared from pristine ($Ni(OH)_2$) and sulfonated ($Ni(OH)_2$-S) nickel hydroxide at different solid concentrations at 298 K; viscosity model fits have been included for comparison; (**b**) viscosity for $Ni(OH)_2$-S nanofluids plotted as a function of temperature; the calibration curve for ethylene glycol has been included as reference, and error bars are also included.

The experimental data for $Ni(OH)_2$-S were compared with various theoretical models to better understand their variation as a function of solid loading. The Einstein–Batchelor model provided describes the viscosity of suspensions containing non-interacting hard spheres (Equation (2)) [26,39,61]:

$$\eta_{relative} = \eta_{nanofluid}/\eta_{base\ fluid} = 1 + 2.5\phi + 6.2\phi^2 \quad (2)$$

where $\eta_{relative}$ is the viscosity of the suspension relative to the base fluid, and ϕ is the volume fraction of solid nanomaterials dispersed in the fluid. Figure 3a shows that the viscosity of $Ni(OH)_2$-S nanofluids appears to be gradually and linearly increasing with solid loading for suspensions with up to 50 wt.%. At higher concentrations, the increase is more rapid, suggesting the presence of strong inter-particle interactions. From Figure 3a, it is clear that the relative viscosity of both $Ni(OH)_2$ and $Ni(OH)_2$-S nanofluids is much higher than that predicted by the basic Einstein–Batchelor model, especially at high (>10 wt.%) mass loading. Other theoretical models include the Kriege–Dougherty relationship, which is a semi-empirical model accounting for a 'crowding effect' that can be expected in concentrated suspensions. Inclusion of such a correction factor or parameter (ϕ_m, the maximum packing fraction) leads to greater sensitivity to incremental changes in concentration. This is defined as the maximum volume of particles that can be added to a suspension before the system becomes jam-packed and viscosity becomes infinite [39,62].

$$\eta_{relative} = \left(1 - \frac{\phi}{\phi_m}\right)^{-[\eta]\phi_m} \quad (3)$$

where $[\eta] = 2.5$ is the intrinsic viscosity.

The Kriege–Dougherty model has been further modified to add an 'effective aggregate' term, ϕ_{agg}, replacing the solid volume fraction (ϕ) term in Equation (3), defined as [39,62]:

$$\phi_{agg} = \phi\left(\frac{a_a}{a}\right)^{3-D_f} \quad (4)$$

where a_a is the radius of the aggregate (which can be determined from dynamic light scattering studies), a is the radius of the particle, and D_f is the fractal dimension of aggre-

gates in the nanofluid with typical values between 1.6 and 2.5. The theoretical values of relative viscosity of these fluids expected from the modified Krieger–Dougherty model are also included in Figure 2a. Assuming D_f = 2.5, the non-linear best fitting yielded a value of ϕ_m = 0.33, which suggests that the concentration of $Ni(OH)_2$-S nanoparticles could potentially be further increased to 67 wt.% (33 vol.%). Variation of the shear rate and its effect on the viscosity of the nanofluids was also explored, though all concentrations exhibited minor changes within ±4 cP (e.g., 60 wt.% from 36 cP at 4 s^{-1} to 32 cP at 100 s^{-1}, Figure S4). Note that this is a considerably lower shear-rate dependence as compared to the study by Brown et al. [59,60], reporting a variation of 1000 cP at 1 s^{-1} to 300 cP at 100 s^{-1}. Furthermore, the shear-dependence in this study is considerably smaller compared to analogous efforts towards aqueous formulations for semi-solid flow batteries using carbon additives [32]. Significant dependence of the viscosity on applied shear rate will have a direct and adverse impact on the pumping power required for flow battery operation [28,32,63].

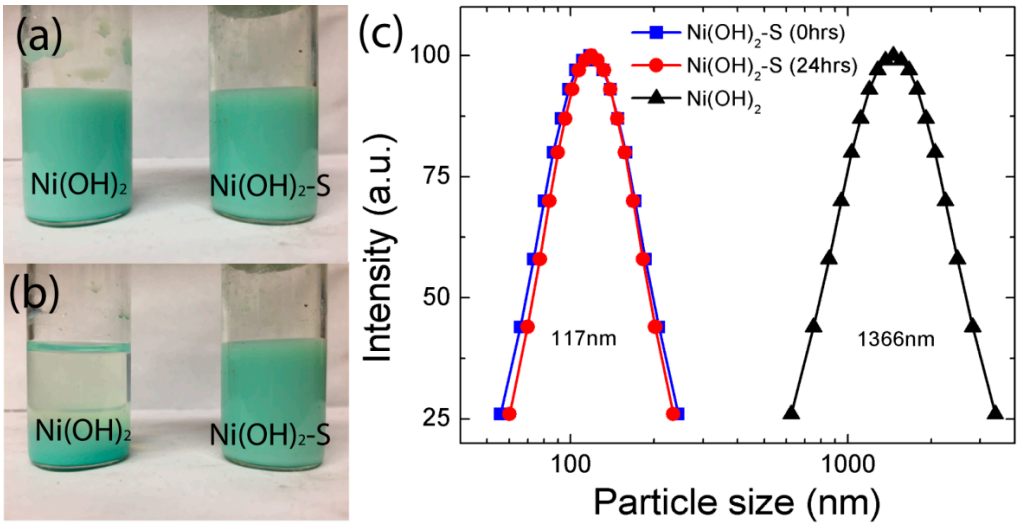

Figure 3. (**a**,**b**) Settling time tests for nanofluids of $Ni(OH)_2$ (**left**) and $Ni(OH)_2$-S (**right**) containing 5 wt% solids (**a**) immediately after ultrasonic processing and (**b**) after 1 week at rest; (**c**) particle size distribution spectra measured with DLS.

3.3. Colloidal Stability of Nanofluids

Colloidal stability is a key factor in the long-term performance of nanofluids. This was evaluated for both $Ni(OH)_2$ and $Ni(OH)_2$-S nanofluids as a settling rate over time. In order to estimate the suspension stability of the nanofluids made from the pristine and modified nanoparticles, photographs were taken at regular intervals of time as settling patterns developed. Figure 3 compares 5 wt.% nanofluids made from pristine $Ni(OH)_2$ and modified $Ni(OH)_2$-S nanoparticles after different intervals of time. The pristine $Ni(OH)_2$ settles soon after the preparation, whereas $Ni(OH)_2$-S remains well dispersed even after weeks at rest. This excellent dispersion stability is attributed to the surface modification, which promotes the separation of the nano-sized particles through both charge and steric-based mechanisms, thereby preventing agglomeration and thus settling.

The state of agglomeration in the nanofluids was studied by dynamic light scattering (DLS), as shown in the number distribution spectra (Figure 3c). The average agglomerate size of the pristine $Ni(OH)_2$ nanofluids was observed to be 1366 nm, compared to the much smaller ~117 nm observed in suspensions of $Ni(OH)_2$-S particles. These contrasting values suggest that the clustering of particles is significant in the case of pristine nanoparticles as they contain large agglomerates with 10–15 times the individual particle diameter. However, suspensions of $Ni(OH)_2$-S particles have excellent dispersion and limited agglomeration since the clusters are restricted to one to two nanoparticle diameters. This smaller cluster size explains the slower rate of gravity-induced settling as well as its superior colloidal

stability. Zeta potential measurements demonstrated values of -30 ± 3 mV for pristine $Ni(OH)_2$ and -48 ± 2 mV for sulfonated $Ni(OH)_2-S$ particles at a pH of 10. The greater value of the zeta potential in $Ni(OH)_2-S$ suspensions further supports the hypothesis of charge-based separation due to negatively charged sulfonate groups and agrees with the observed enhancement in colloidal stability of $Ni(OH)_2-S$ suspensions. Dynamic light scattering and zeta potential results further demonstrate the nanoparticle's ability to disperse in a particular liquid and remain separated, although such measurements are limited to dilute concentrations.

3.4. Thermal Conductivity of Nanofluids

Thermal conductivities of nanofluids containing both $Ni(OH)_2$ and $Ni(OH)_2$-S particles were determined to understand the effects of surface modification and high particle loading. The results (Figure 4) are reported as an enhancement in thermal conductivity for both $Ni(OH)_2$ and $Ni(OH)_2$-S as a function of nanoparticle concentration. Values reported are relative to the base fluid value, which was measured to be 0.587 $Wm^{-1}K^{-1}$ at ambient room temperature.

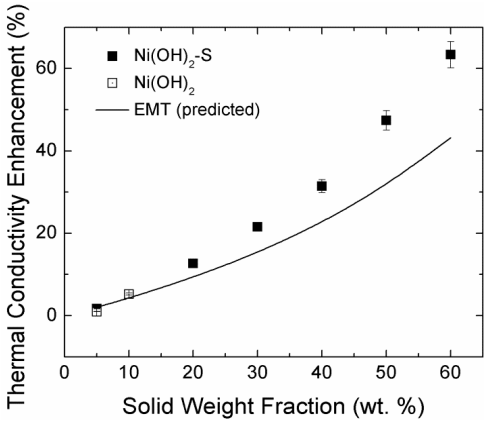

Figure 4. Changes in thermal conductivity over base fluid as a function of solid weight fraction at room temperature for both $Ni(OH)_2$ and $Ni(OH)_2$-S; values predicted by theoretical models (EMT, solid line) are included for comparison.

Theoretical models such as the effective medium theory (EMT) is typically used for predicting the thermal conductivity of nanofluids with ceramic particles [47].

$$\frac{k_{nf}}{k_0} = 1 + 3(k_p - k_0)\phi/(k_p + 2k_0) \quad (5)$$

where ϕ is the volume fraction of solid particles, k_{nf}, k_p and k_0 are the thermal conductivity for the nanofluid, solid particles and base fluid, respectively. Literature reports on the thermal properties of nickel hydroxide nanoparticles are limited, and hence, a value of k_p = 20.2 $Wm^{-1}K^{-1}$ for nickel oxide was used as a close approximation [64,65]. EMT-predicted values of the thermal conductivity enhancement are plotted in Figure 4 using the conversion of volume to mass fraction, as described in the supporting information (Figure S1).

At low solid loadings (5 and 10 wt.%), experimental results for thermal conductivity of both pristine $Ni(OH)_2$ and $Ni(OH)_2$-S nanofluids show values similar to those predicted by EMT. At higher solid loading (20 wt.%), the experimental thermal conductivity is slightly higher than the EMT prediction, likely due to the successively increasing degree of agglomeration that provides more effective, extended paths for heat conduction within solid particle ensembles rather than solid/liquid/solid paths. For the nanofluids with particle concentration below the aggregation threshold, e.g., 5 and 10 wt.%, the surface modification does not appear to have a significant effect on thermal conductivity since similar values

were seen for both $Ni(OH)_2$ and $Ni(OH)_2$-S. Thermal conductivity enhancements as high as 64% were observed for a solid loading of 60 wt.% (26 vol.%) as compared to 43% expected from EMT. The relatively close agreement between experimental and EMT-predicted values of thermal conductivity of $Ni(OH)_2$-S nanofluids serves as an additional confirmation of the critical role of the surface treatment on the agglomeration state of nanoparticles.

3.5. Electrochemical Testing

Solid-casted electrodes with two nanoparticle materials were tested in a concentrated aqueous alkali electrolyte, as shown in Figure 5. CV of the pristine $Ni(OH)_2$ sample exhibited a sharp feature at 0.53V, likely related to a redox process at a particulate crystallographic plane, followed by a broad oxidation peak. Oxidation of the $Ni(OH)_2$-S sample does not exhibit such a sharp feature (red curve) but has a small pre-peak at ~0.43V. Redox peak positions in $Ni(OH)_2$-S were shifted by 20 mV closer to the equilibrium potential, indicating better reversibility compared to the pristine sample. However, the discharge capacity (Figure 5c) of the surface-modified sample (237 mAh/g) was observed to be ~15% less than pristine $Ni(OH)_2$ (275 mAh/g), which is very close to the theoretical capacity of this material (289 mAh/g). Continuous cycling (Figure 5c) shows a consistent activation in initial cycles for both pristine and modified materials but with better stability of the surface-modified material over the course of 50 repeated charge–discharge cycles. The lower discharge capacity of the surface-modified material as compared to the pristine can likely be attributed to the additional barrier to charge transfer created by the silane coating. However, this needs to be further studied to explore the role of the thickness of the silane layer, which is not redox-active, and how it may interfere with electron transfer kinetics to and from the underlying nanoparticle.

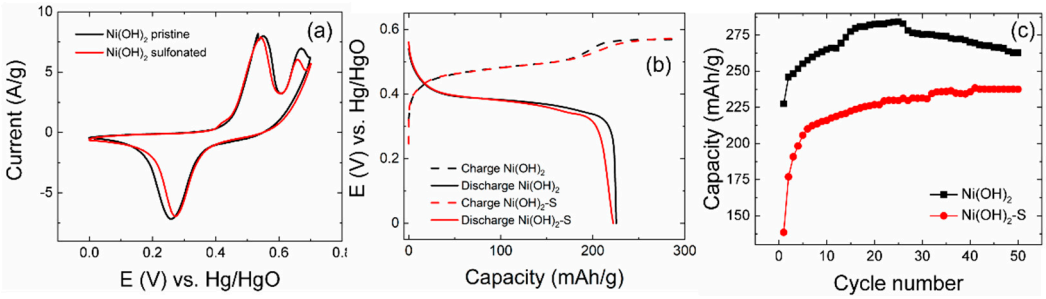

Figure 5. Electrochemical tests of pristine $Ni(OH)_2$ and sulfonated $Ni(OH)_2$-S nanoparticles in the form of solid casted electrodes in concentrated aqueous hydroxide electrolyte. (**a**) Cyclic voltammograms (CV) performed at a scan rate of 1 mV/s; (**b**) charge (C/3) and discharge curves (C/6); (**c**) discharge capacity as a function of cycling number.

4. Conclusions

This study reports a novel approach toward the development of nanofluids containing nickel hydroxide nanoparticles with high solid loading, low viscosity and good electrochemical activity. An optimized procedure was developed and demonstrated for the surface grafting of small organosilane-based molecules with negatively charged sulfonate groups onto β-$Ni(OH)_2$ nanoparticles. The total fraction of grafting moiety in the modified material was found to be <3 wt.% by thermogravimetric analysis. Surface modification of β-$Ni(OH)_2$ nanoparticles enabled the formulation of very stable dispersions with over 60 wt.% (26 vol.%) of solids in alkaline aqueous electrolytes, with a modest viscosity of ~32 cP at 298 K. For comparison, nanofluids from pristine β-$Ni(OH)_2$ nanoparticles showed paste-like consistency at solid loadings of 10 wt.% (2.6 vol.%). Nanofluids with modified nanoparticles exhibit up to 64% enhancement in thermal conductivity when compared to the base electrolyte, which is linearly proportional to volumetric particle concentration. Suspension stability and low viscosity of nanofluids with surface-modified nanoparticles were correlated to the limited nanoparticle agglomeration, as indicated by dynamic light

scattering results. Electrochemical testing as solid casted electrodes showed a maximum reversible discharge capacity of approximately 275 mAh/g for pristine and 237 mAh/g for surface-modified electrodes, indicating that ~15% of electrochemical activity of nanoparticles is suppressed after the surface modification procedure, but the $Ni(OH)_2$-S electrode showed more stable performance over 50 cycles. Future studies will further examine the long-term electrochemical cycling behavior, thermal and chemical stability of the surface graft under relevant experimental conditions and performance in suspension-type nanofluid electrodes at different particle concentrations and ionic strengths.

Supplementary Materials: The following supporting information can be downloaded at: https://www.mdpi.com/article/10.3390/en15134728/s1, Figure S1: Graphical depiction of the relationship between weight and volume fraction for nickel (II) hydroxide nanofluids in water; Figure S2: SEM images of (a) pristine nickel (II) hydroxide nanoparticles ($Ni(OH)_2$) and (b) sulfonated nickel hydroxide nanoparticles ($Ni(OH)_2$-S); Figure S3: XRD patterns of pristine nickel (II) hydroxide nanoparticles ($Ni(OH)_2$) and sulfonated nickel hydroxide nanoparticles ($Ni(OH)_2$-S); Figure S4: Variation in viscosity as a function of (a) shear stress and (b) shear rate for sulfonated nickel hydroxide nanofluids at room temperature (with torque >10% and <90%).

Author Contributions: Conceptualization, S.S. and E.V.T.; methodology, S.S. and E.V.T.; investigation and validation, S.S., E.M., S.A., E.D., C.U.S. and E.V.T.; writing—original draft preparation, S.S.; writing—review and editing, S.S., E.D. and E.V.T.; project administration, C.U.S. and E.V.T. All authors have read and agreed to the published version of the manuscript.

Funding: This research was funded in part by NASA 80AFRC19C0004 contract and the U.S. Department of Energy, Advanced Research Funding Agency-Energy (ARPAE) under award AR000387.

Institutional Review Board Statement: Not applicable.

Informed Consent Statement: Not applicable.

Data Availability Statement: The data presented in this study are available on request from the corresponding author.

Conflicts of Interest: The authors declare no conflict of interest.

References

1. Buongiorno, J.; Venerus, D.C.; Prabhat, N.; McKrell, T.; Townsend, J.; Christianson, R.; Tolmachev, Y.V.; Keblinski, P.; Hu, L.W.; Alvarado, J.L.; et al. A benchmark study on the thermal conductivity of nanofluids. *J. Appl. Phys.* **2009**, *106*, 094312. [CrossRef]
2. Cingarapu, S.; Singh, D.; Timofeeva, E.V.; Moravek, M.R. Nanofluids with encapsulated tin nanoparticles for advanced heat transfer and thermal energy storage. *Int. J. Energy Res.* **2014**, *38*, 51–59. [CrossRef]
3. Yu, W.; France, D.M.; Timofeeva, E.V.; Singh, D. Effective Thermal Conductivity Models for Carbon Nanotube-Based Nanofluids. *J. Nanofluids* **2013**, *2*, 69–73. [CrossRef]
4. Raja, M.; Vijayan, R.; Dineshkumar, P.; Venkatesan, M. Review on nanofluids characterization, heat transfer characteristics and applications. *Renew. Sustain. Energy Rev.* **2016**, *64*, 163–173. [CrossRef]
5. Babita; Sharma, S.K.; Gupta, S.M. Preparation and evaluation of stable nanofluids for heat transfer application: A review. *Exp. Therm. Fluid Sci.* **2016**, *79*, 202–212.
6. Akhavan-Behabadi, M.A.; Shahidi, M.; Aligoodarz, M.R.; Fakoor-Pakdaman, M. An experimental investigation on rheological properties and heat transfer performance of MWCNT-water nanofluid flow inside vertical tubes. *Appl. Therm. Eng.* **2016**, *106*, 916–924. [CrossRef]
7. Rueda-García, D.; Rodríguez-Laguna, M.d.R.; Chávez-Angel, E.P.; Dubal, D.; Cabán-Huertas, Z.; Benages-Vilau, R.; Gómez-Romero, P. From Thermal to Electroactive Graphene Nanofluids. *Energies* **2019**, *12*, 4545. [CrossRef]
8. Rueda-Garcia, D.; Caban-Huertas, Z.; Sanchez-Ribot, S.; Marchante, C.; Benages, R.; Dubal, D.P.; Ayyad, O.; Gomez-Romero, P. Battery and supercapacitor materials in flow cells. Electrochemical energy storage in a $LiFePO_4$/reduced graphene oxide aqueous nanofluid. *Electrochim. Acta* **2018**, *281*, 594–600. [CrossRef]
9. Dubal, D.P.; Gomez-Romero, P. Electroactive graphene nanofluids for fast energy storage. *2D Mater.* **2016**, *3*, 031004. [CrossRef]
10. Dubal, D.P.; Rudea-Garcia, D.; Marchante, C.; Benages, R.; Gomez-Romero, P. Hybrid Graphene-Polyoxometalates Nanofluids as Liquid Electrodes for Dual Energy Storage in Novel Flow Cells. *Chem. Rec.* **2018**, *18*, 1076–1084. [CrossRef]
11. Souza, R.R.; Gonçalves, I.M.; Rodrigues, R.O.; Minas, G.; Miranda, J.M.; Moreira, A.L.N.; Lima, R.; Coutinho, G.; Pereira, J.E.; Moita, A.S. Recent advances on the thermal properties and applications of nanofluids: From nanomedicine to renewable energies. *Appl. Therm. Eng.* **2022**, *201*, 117725. [CrossRef]

12. Liu, C.; Qiao, Y.; Du, P.; Zhang, J.; Zhao, J.; Liu, C.; Huo, Y.; Qi, C.; Rao, Z.; Yan, Y. Recent advances of nanofluids in micro/nano scale energy transportation. *Renew. Sustain. Energy Rev.* **2021**, *149*, 111346. [CrossRef]
13. Gang, Q.; Wang, R.-T.; Wang, J.-C. Estimations on Properties of Redox Reactions to Electrical Energy and Storage Device of Thermoelectric Pipe (TEP) Using Polymeric Nanofluids. *Polymers* **2021**, *13*, 1812. [CrossRef] [PubMed]
14. Aberoumand, S.; Woodfield, P.; Shabani, B.; Dao, D.V. Advances in electrode and electrolyte improvements in vanadium redox flow batteries with a focus on the nanofluidic electrolyte approach. *Phys. Rep.* **2020**, *881*, 1–49. [CrossRef]
15. Bharathidasan, P.; Subramaniam, T.; Chandini, D.; Sivakkumar, S.R.; Rajan, K.S.; Devaraj, S. Simultaneous Enhancement of Energy and Power Density of Reduced Graphene Oxide by the Effect of Dispersed Metal Oxide Nanoparticles in the Electrolyte. *J. Electrochem. Soc.* **2020**, *167*, 140524. [CrossRef]
16. Joseph, A.; Xavier, M.M.; Fal, J.; Żyła, G.; Sasi, S.; Radhakrishnan Nair, P.; Padmanabhan, A.S.; Mathew, S. Synthesis and electrochemical characterization of electroactive IoNanofluids with high dielectric constants from hydrated ferrous sulphate. *J. Chem. Soc. Chem. Commun.* **2019**, *55*, 83–86. [CrossRef]
17. Kim, J.; Park, H. Synergistic effect of nanofluid as catalyst with carbon foam electrode for improved rheological properties of aqueous electrolytes for vanadium redox flow battery. *J. Power Sources* **2021**, *500*, 229974. [CrossRef]
18. Said, Z.; Allagui, A.; Abdelkareem, M.A.; Alawadhi, H.; Elsaid, K. Acid-functionalized carbon nanofibers for high stability, thermoelectrical and electrochemical properties of nanofluids. *J. Colloid Interface Sci.* **2018**, *520*, 50–57. [CrossRef]
19. Seed, C.M.; Acharya, B.; Perelygin, V.; Smirnov, A.I.; Krim, J. Tribotronic control and cyclic voltammetry of platinum interfaces with metal oxide nanofluids. *Appl. Surf. Sci.* **2021**, *566*, 150675. [CrossRef]
20. Zapata-Hernandez, C.; Durango-Giraldo, G.; López, D.; Buitrago-Sierra, R.; Cacua, K. Surfactants versus surface functionalization to improve the stability of graphene nanofluids. *J. Dispers. Sci. Technol.* **2021**, 1–8. [CrossRef]
21. Losev, A.V.; Petrii, O.A.; Nauki, I. Suspension and fluidized electrodes. *Electrokhimiya* **1979**, *14*, 120.
22. Aberoumand, S.; Woodfield, P.; Shi, G.; Kien Nguyen, T.; Nguyen, H.-Q.; Li, Q.; Shabani, B.; Viet Dao, D. Thermo-electro-rheological behaviour of vanadium electrolyte-based electrochemical graphene oxide nanofluid designed for redox flow battery. *J. Mol. Liq.* **2021**, *338*, 116860. [CrossRef]
23. Jung Lee, H.; Bai, S.-J.; Seok Song, Y. Microfluidic Electrochemical Impedance Spectroscopy of Carbon Composite Nanofluids. *Sci. Rep.* **2017**, *7*, 722. [CrossRef]
24. Ghosh, S.; Subudhi, S. Developments in fuel cells and electrochemical batteries using nanoparticles and nanofluids. *Energy Storage* **2021**, *4*, e288. [CrossRef]
25. Sokolov, S.V.; Kätelhön, E.; Compton, R.G. Near-Wall Hindered Diffusion in Convective Systems: Transport Limitations in Colloidal and Nanoparticulate Systems. *J. Phys. Chem. C* **2016**, *120*, 10629–10640. [CrossRef]
26. Sen, S.; Chow, C.-M.; Moazzen, E.; Segre, C.U.; Timofeeva, E.V. Electroactive nanofluids with high solid loading and low viscosity for rechargeable redox flow batteries. *J. Appl. Electrochem.* **2017**, *47*, 593–605. [CrossRef]
27. Alotto, P.; Guarnieri, M.; Moro, F. Redox flow batteries for the storage of renewable energy: A review. *Renew. Sustain. Energy Rev.* **2014**, *29*, 325–335. [CrossRef]
28. Timofeeva, E.V.; Katsoudas, J.P.; Segre, C.U.; Singh, D. Rechargeable Nanofluid Electrodes for High Energy Density Flow Battery, Cleantech 2013, Chapter 9, Energy Storage. pp. 363–366. Available online: https://briefs.techconnect.org/wp-506content/volumes/Cleantech2013/pdf/535.pdf (accessed on 22 June 2022).
29. Weber, A.Z.; Mench, M.M.; Meyers, J.P.; Ross, P.N.; Gostick, J.T.; Liu, Q. Redox flow batteries: A review. *J. Appl. Electrochem.* **2011**, *41*, 1137. [CrossRef]
30. Garche, J.; Dietz, H.; Wiesener, K. The suspension electrode technique for electrochemical analysis of lead dioxide. *J. Electroanal. Chem. Interfacial Electrochem.* **1984**, *180*, 577–585. [CrossRef]
31. Duduta, M.; Ho, B.; Wood, V.C.; Limthongkul, P.; Brunini, V.E.; Carter, W.C.; Chiang, Y.-M. Semi-Solid Lithium Rechargeable Flow Battery. *Adv. Energy Mater.* **2011**, *1*, 511–516. [CrossRef]
32. Li, Z.; Smith, K.C.; Dong, Y.; Baram, N.; Fan, F.Y.; Xie, J.; Limthongkul, P.; Carter, W.C.; Chiang, Y.-M. Aqueous semi-solid flow cell: Demonstration and analysis. *Phys. Chem. Chem. Phys.* **2013**, *15*, 15833–15839. [CrossRef] [PubMed]
33. Boota, M.; Hatzell, K.B.; Alhabeb, M.; Kumbur, E.C.; Gogotsi, Y. Graphene-containing flowable electrodes for capacitive energy storage. *Carbon* **2015**, *92*, 142–149. [CrossRef]
34. Hatzell, K.B.; Fan, L.; Beidaghi, M.; Boota, M.; Pomerantseva, E.; Kumbur, E.C.; Gogotsi, Y. Composite Manganese Oxide Percolating Networks as a Suspension Electrode for an Asymmetric Flow Capacitor. *ACS Appl. Mater. Interfaces* **2014**, *6*, 8886–8893. [CrossRef] [PubMed]
35. Su, P.; Zhang, H.; Yang, L.; Xing, C.; Pan, S.; Lu, W.; Zhang, S. Effects of conductive additives on the percolation networks and rheological properties of $LiMn_{0.7}Fe_{0.3}PO_4$ suspensions for lithium slurry battery. *Chem. Eng. J.* **2022**, *433*, 133203. [CrossRef]
36. Wilk, J.; Grosicki, S. Limiting current technique in the research of mass/heat transfer in nanofluid. *J. Phys. Conf. Ser.* **2016**, *745*, 032084. [CrossRef]
37. Meethong, N.; Huang, H.-Y.S.; Carter, W.C.; Chiang, Y.-M. Size-Dependent Lithium Miscibility Gap in Nanoscale $Li_{1-x}FePO_4$. *Electrochem. Solid-State Lett.* **2007**, *10*, A134. [CrossRef]
38. Sen, S.; Moazzen, E.; Aryal, S.; Segre, C.U.; Timofeeva, E.V. Engineering nanofluid electrodes: Controlling rheology and electrochemical activity of γ-Fe_2O_3 nanoparticles. *J. Nanopart. Res.* **2015**, *17*, 437. [CrossRef]

39. Sen, S.; Govindarajan, V.; Pelliccione, C.J.; Wang, J.; Miller, D.J.; Timofeeva, E.V. Surface Modification Approach to TiO_2 Nanofluids with High Particle Concentration, Low Viscosity, and Electrochemical Activity. *ACS Appl. Mater. Interfaces* **2015**, *7*, 20538–20547. [CrossRef]
40. Hall, D.S.; Lockwood, D.J.; Bock, C.; MacDougall, B.R. Nickel hydroxides and related materials: A review of their structures, synthesis and properties. *Proc. R. Soc. A* **2015**, *471*, 20140792. [CrossRef]
41. Zhao, Y.; Zhao, B.; Liu, J.; Chen, G.; Gao, R.; Yao, S.; Li, M.; Zhang, Q.; Gu, L.; Xie, J.; et al. Oxide-Modified Nickel Photocatalysts for the Production of Hydrocarbons in Visible Light. *Angew. Chem. Int. Ed.* **2016**, *55*, 4215–4219. [CrossRef]
42. Gao, M.; Sheng, W.; Zhuang, Z.; Fang, Q.; Gu, S.; Jiang, J.; Yan, Y. Efficient Water Oxidation Using Nanostructured α-Nickel-Hydroxide as an Electrocatalyst. *J. Am. Chem. Soc.* **2014**, *136*, 7077–7084. [CrossRef] [PubMed]
43. Chen, H.; Hu, L.; Yan, Y.; Che, R.; Chen, M.; Wu, L. One-Step Fabrication of Ultrathin Porous Nickel Hydroxide-Manganese Dioxide Hybrid Nanosheets for Supercapacitor Electrodes with Excellent Capacitive Performance. *Adv. Energy Mater.* **2013**, *3*, 1636–1646. [CrossRef]
44. Singu, B.S.; Male, U.; Hong, S.E.; Yoon, K.R. Synthesis and performance of nickel hydroxide nanodiscs for redox supercapacitors. *Ionics* **2016**, *22*, 1485–1491. [CrossRef]
45. Mao, L.; Guan, C.; Huang, X.; Ke, Q.; Zhang, Y.; Wang, J. 3D Graphene-Nickel Hydroxide Hydrogel Electrode for High-Performance Supercapacitor. *Electrochim. Acta* **2016**, *196*, 653–660. [CrossRef]
46. Zhu, Y.; Cao, C.; Tao, S.; Chu, W.; Wu, Z.; Li, Y. Ultrathin Nickel Hydroxide and Oxide Nanosheets: Synthesis, Characterizations and Excellent Supercapacitor Performances. *Sci. Rep.* **2014**, *4*, 5787. [CrossRef] [PubMed]
47. Parveen, N.; Cho, M.H. Self-Assembled 3D Flower-Like Nickel Hydroxide Nanostructures and Their Supercapacitor Applications. *Sci. Rep.* **2016**, *6*, 27318. [CrossRef] [PubMed]
48. Sialvi, M.Z.; Mortimer, R.J.; Wilcox, G.D.; Teridi, A.M.; Varley, T.S.; Wijayantha, K.G.U.; Kirk, C.A. Electrochromic and Colorimetric Properties of Nickel(II) Oxide Thin Films Prepared by Aerosol-Assisted Chemical Vapor Deposition. *ACS Appl. Mater. Interfaces* **2013**, *5*, 5675–5682. [CrossRef]
49. Sonavane, A.C.; Inamdar, A.I.; Shinde, P.S.; Deshmukh, H.P.; Patil, R.S.; Patil, P.S. Efficient electrochromic nickel oxide thin films by electrodeposition. *J. Alloys Compod.* **2010**, *489*, 667–673. [CrossRef]
50. Fantini, M.; Gorenstein, A. Electrochromic nickel hydroxide films on transparent/conducting substrates. *Sol. Energy Mater.* **1987**, *16*, 487–500. [CrossRef]
51. Wen, R.-T.; Niklasson, G.A.; Granqvist, C.G. Electrochromic nickel oxide films and their compatibility with potassium hydroxide and lithium perchlorate in propylene carbonate: Optical, electrochemical and stress-related properties. *Thin Solid Films* **2014**, *565*, 128–135. [CrossRef]
52. Mathew, M.; Sandhyarani, N. A highly sensitive electrochemical glucose sensor structuring with nickel hydroxide and enzyme glucose oxidase. *Electrochim. Acta* **2013**, *108*, 274–280. [CrossRef]
53. Canevari, T.C.; Cincotto, F.H.; Landers, R.; Machado, S.A.S. Synthesis and characterization of α-nickel (II) hydroxide particles on organic-inorganic matrix and its application in a sensitive electrochemical sensor for vitamin D determination. *Electrochim. Acta* **2014**, *147*, 688–695. [CrossRef]
54. Yang, H.; Gao, G.; Teng, F.; Liu, W.; Chen, S.; Ge, Z. Nickel Hydroxide Nanoflowers for a Nonenzymatic Electrochemical Glucose Sensor. *J. Electrochem. Soc.* **2014**, *161*, B216–B219. [CrossRef]
55. Gangwar, J.; Dey, K.K.; Tripathi, S.K.; Wan, M.; Yadav, R.R.; Singh, R.K.; Samta; Srivastava, A.K. NiO-based nanostructures with efficient optical and electrochemical properties for high-performance nanofluids. *Nanotechnology* **2013**, *24*, 415705. [CrossRef]
56. Qazi, S.J.S.; Rennie, A.R.; Cockcroft, J.K.; Vickers, M. Use of wide-angle X-ray diffraction to measure shape and size of dispersed colloidal particles. *J. Colloid Interface Sci.* **2009**, *338*, 105–110. [CrossRef]
57. Qazi, S.J.S.; Rennie, A.R.; Tucker, I.; Penfold, J.; Grillo, I. Impact of $Ni(OH)_2$ Platelike Particles on Lamellar Surfactant Mesophases and the Orientation of Their Mixtures under Elongational Flow. *J. Phys. Chem. B* **2011**, *115*, 10413–10424. [CrossRef]
58. Qazi, S.J.S.; Karlsson, G.; Rennie, A.R. Self-Assembled Structures of Disc-Like Colloidal Particles. In *Trends in Colloid and Interface Science XXIV*; Springer: Berlin/Heidelberg, Germany, 2011.
59. Brown, A.B.D.; Clarke, S.M.; Rennie, A.R. Ordered Phase of Platelike Particles in Concentrated Dispersions. *Langmuir* **1998**, *14*, 3129–3132. [CrossRef]
60. Brown, A.B.D.; Ferrero, C.; Narayanan, T.; Rennie, A.R. Phase separation and structure in a concentrated colloidal dispersion of uniform plates. *Eur. Phys. J. B* **1999**, *11*, 481–489. [CrossRef]
61. Utomo, A.T.; Poth, H.; Robbins, P.T.; Pacek, A.W. Experimental and theoretical studies of thermal conductivity, viscosity and heat transfer coefficient of titania and alumina nanofluids. *Int. J. Heat Mass Transfer* **2012**, *55*, 7772–7781. [CrossRef]
62. Using The Krieger−Dougherty Model to Predict Suspension, Viscosity. *Technical Note, Version 5, Malvern Instruments*. Available online: http://www.malvern.com/ (accessed on 22 June 2022).
63. Routbort, J.L.; Singh, D.; Timofeeva, E.V.; Yu, W.; France, D.M. Pumping power of nanofluids in a flowing system. *J. Nanopart. Res.* **2011**, *13*, 931–937. [CrossRef]
64. Slack, G.A.; Newman, R. Thermal Conductivity of MnO and NiO. *Phys. Rev. Lett.* **1958**, *1*, 359–360. [CrossRef]
65. Keem, J.E.; Honig, J.M. Selected Electrical and Thermal Properties of Undoped Nickel Oxide. 1978, 578. Available online: https://apps.dtic.mil/sti/citations/ADA128940 (accessed on 22 June 2022).